Journal of Materials Chemistry C

PAPER

View Article Online
View Journal | View Issue

Cite this: J. Mater. Chem. C, 2014, 2, 7392

Individual HfS_3 nanobelt for field-effect transistor and high performance visible-light detector

Wei-Wei Xiong, Jin-Qiang Chen, Xing-Cai Wu* and Jun-Jie Zhu*

Received 19th May 2014
Accepted 9th July 2014

DOI: 10.1039/c4tc01039f

www.rsc.org/MaterialsC

HfS_3 nanobelts were directly synthesized *via* a simple chemical vapor transport method. A field-effect transistor and photodetector was further fabricated based on an individual HfS_3 nanobelt, and its electrical and optoelectronic properties were evaluated. The output characteristic curves of the FET revealed a typical p-type semiconducting behavior. The photodetector has an ultralow dark current (0.04 pA) and a large on/off ratio (337.5) illuminated by 405 nm light with 1.2 mW cm^{-2}. It demonstrated excellent stability and sensitivity to 405 nm light. The results suggest that the HfS_3 nanobelts are promising for application in nanoscale electronic and optoelectronic devices. The research will play a positive role in nanodevice research of one-dimensional transition-metal trichalcogenide nanostructure.

Introduction

Over the past decades, one-dimensional (1D) transition metal chalcogenide nanostructure materials, such as nanowires,[1,2] nanorods,[3] nanotubes and nanobelts,[4–7] have been widely studied, and considerable efforts have been devoted to explore the novel phenomena and investigate the distinctive properties. Due to their large surface-to-volume ratios and reduced dimensionality,[8] 1D transition-metal chalcogenides can be used by themselves in electronic and optical nanodevices, such as gas sensors,[9] light emission diodes,[10] field emitters,[6,7] solar cells,[11] field-effect transistors (FETs) and photodetectors.[2,5,8]

HfS_3 nanobelts are semiconducting materials belonging to the family of trichalcogenides of group IV transition metals, which are characterized by a chain-like and layered-type structure.[12] HfS_3 grow as needle or fiber-like crystals with each metal atom located at the center of a trigonal prism of sulfur atoms that are arranged in chains along the *b* axis of the monoclinic structure. Neighboring chains are offset by *b*/2 and connected laterally into sheets through metal–chalcogen bonds; the layers are hold together by weak van der Waals forces.[13] Different from other transition metal chalcogenides, the chemical and physical properties of HfS_3 have rarely been studied except for a few theoretical researches.[13,14] Group IV transition metal chalcogenides with energy band gaps covering the visible spectral range are candidates for nano-optoelectronic devices. Recently, TiS_3, ZrS_3 and ZrS_2 nanobelts were synthesized in our group and proved to have excellent field emission performances.[15,16] In the following studies, Li *et al.* demonstrated the well applications of ZrS_2 nanobelts in photodetectors and solar cells for the first time.[17,18] Therefore, investigation into HfS_3 nanobelt devices would push forward our cognition and the practical applications of HfS_3 nanobelts.

Herein, we report for the first time the fabrication of electronic and optoelectronic devices based on individual HfS_3 nanobelts that were synthesized by a chemical vapor transport method.

Results and discussion

The powder X-ray diffraction (XRD) pattern of the sample obtained at 650 °C is shown in Fig. 1a, which corresponds to pure HfS_3 with a monoclinic system (JCPDS no. 65-2348). The morphology of the HfS_3 nanobelts was examined by scanning electron microscopy (SEM) images, as shown in Fig. 1b and c, revealing the formation of 1D belt-like nanostructure with diameter of 300–500 nm, lengths of several tens of micrometers, as well as smooth surfaces. The energy dispersive X-ray spectroscopy (EDS) spectrum of the HfS_3 nanobelts is presented in Fig. 1d, indicating that the product composition is close to the stoichiometry of HfS_3 (Hf : S = 26.93 : 73.07 ≈ 1 : 3). The detailed structures and orientation of the nanobelts were studied by transmission electron microscopy (TEM) and selected areas electron diffraction (SAED). The TEM image at low magnification (Fig. 1e) displays the belt-like structure with smooth surfaces. The high-resolution TEM (HRTEM) image shows uniform structure and clear lattice fringe. As shown in Fig. 2f, the fringe spacing of the HfS_3 nanobelt is 0.51 nm, corresponding to the *d*-value [100] of the monoclinic structure. The electron diffraction analysis confirmed that the nanobelts were single crystals with [100] lateral direction and [010] growth orientation.[13]

To construct an individual HfS_3 nanobelt-based device, the HfS_3 nanobelts were dispersed in ethanol and dropped on a

School of Chemistry and Chemical Engineering, Key Laboratory of Mesoscopic Chemistry of MOE, State Key Lab. of Analytical Chemistry for Life Science, Nanjing University, Nanjing, 210093, P. R. China. E-mail: wuxingca@nju.edu.cn; jjzhu@nju.edu.cn; Fax: +86-25-83597204; Tel: +86-25-83597204

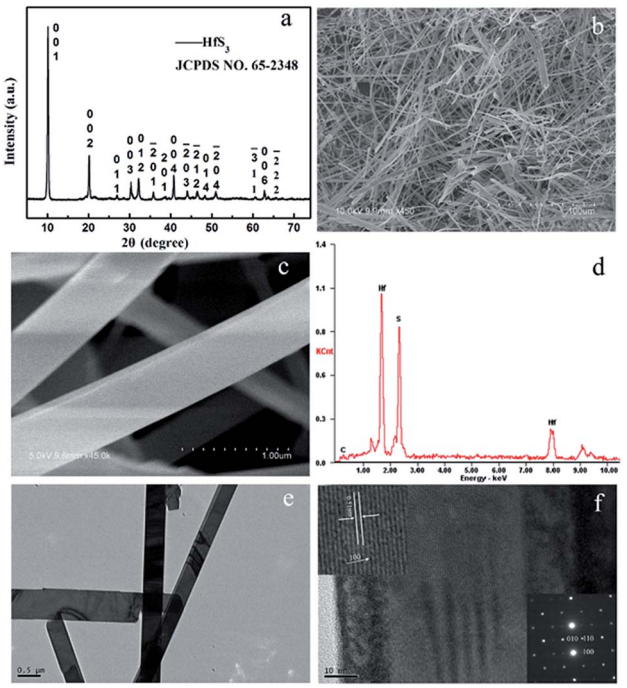

Fig. 1 (a) X-ray diffraction pattern of the HfS_3 nanobelts. (b and c) SEM images of the HfS_3 nanobelts. (d) Energy dispersive X-ray spectroscopy analysis of the HfS_3 nanobelts. (e) TEM images of the HfS_3 nanobelts. (f) HRTEM and SAED images of the HfS_3 nanobelts.

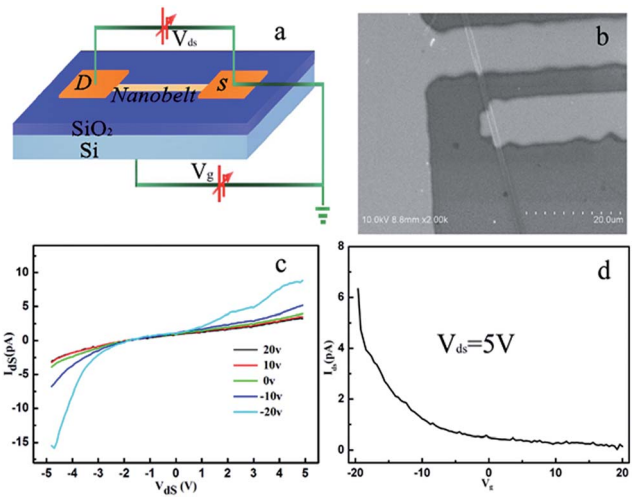

Fig. 2 (a) FET schematic of an individual HfS_3-nanobelt. (b) SEM image of the individual nanobelt FET. (c) Output characteristics I_{ds}–V_{ds} of the single HfS_3 nanobelt FET. (d) The gate transfer characteristic I_{ds}–V_g of the individual nanobelt at $V_{ds} = 5.0$ V.

SiO_2/Si substrate. The patterned Ti (10 nm)/Au (100 nm) electrodes were deposited on the substrate, which was sparsely covered by the HfS_3 nanobelts using photolithography, electron-beam deposition and the lift-off process. Fig. 2a represents a schematic illustration of HfS_3 nanobelt FET, and a SEM image of an individual FET is shown in Fig. 2b. The width of the HfS_3 nanobelt and gap between the two electrodes are around 1.3 μm and 6.4 μm, respectively. Fig. 2c presents the source-drain current (I_{ds}) *versus* source-drain voltage (V_{ds}) curves obtained under gate voltages (V_g) varying from −20 to 20 V. It can be found that for all V_g, I_{ds} increases with increasing V_g, suggesting typical p-type semiconductors characteristics.[19] The transit characteristic curve of the HfS_3 nanobelt FET at $V_{ds} = 5$ V, is shown in Fig. 2d. From the linear region of the curve, the threshold gate voltage (V_{th}) and the transconductance $g_m = dI_{ds}/dV_g$ are determined to be −9.9 V and 5.08×10^{-4} nS, respectively.

To investigate the photoelectric properties, the dc conductance under monochromatic light of different wavelengths was measured on the FET device without applying a gate voltage. Fig. 3a and Fig. 3b present the schematic of HfS_3-nanobelt photodetectors device and SEM image of a single-nanobelt, respectively. Fig. 3c compares the *I*–*V* curves of the photodetector exposed to the light of different wavelengths (405 nm, 532 nm, 650 nm) and under dark conditions. The device showed an ultralow dark current of 0.04 pA at an applied voltage of 5.0 V. There was only small change in the photoresponsivity when the wavelengths of the light source were 650 nm and 532 nm. While the device was illuminated by 405 nm light at 1.2 mW cm^{-2}, the photocurrent dramatically increased by nearly 34.8 times and 7.9 times than 532 nm (1.93 pA) and 650 nm (0.44 pA) at applied voltage of −5.0 V, respectively. This is also consistent with the UV-vis absorption spectrum with maximum absorption at 405 nm as shown in Fig. 3d. Therefore, the results suggest that the HfS_3 nanobelt photodectector have good sensitivity and high selectivity. Furthermore, the non-linear *I*–*V* curves were likely due to the formation of a Schottky barrier between the Ti/Au electrode and the HfS_3 nanobelt.[20]

The responses of the device under different working atmospheres were also investigated, as illustrated in Fig. 4a. The photocurrent of the device measured in air condition was 15.30 pA, about 11.5 times higher than that in vacuum (1.29 pA) or nitrogen (1.35 pA) conditions at applied voltage of −5 V. This

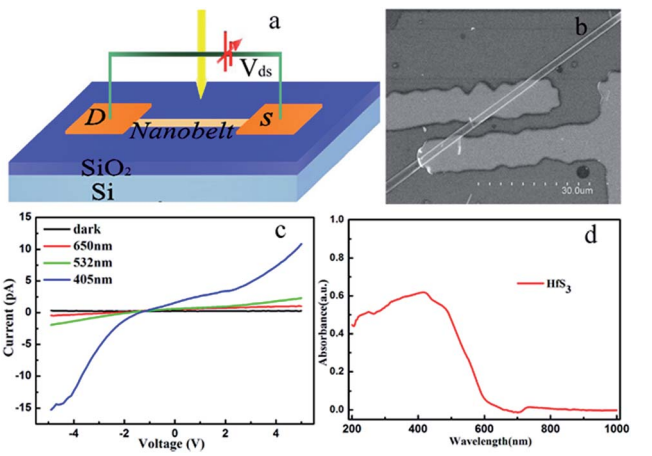

Fig. 3 (a) Schematic illustration of the HfS_3 nanobelt photodetector. (b) A typical SEM image of the photodetector. (c) The *I*–*V* characteristics of an HfS_3 nanobelt photodetector illuminated with different wavelength light and dark condition. (d) The UV-vis absorption spectrum of HfS_3 nanobelts.

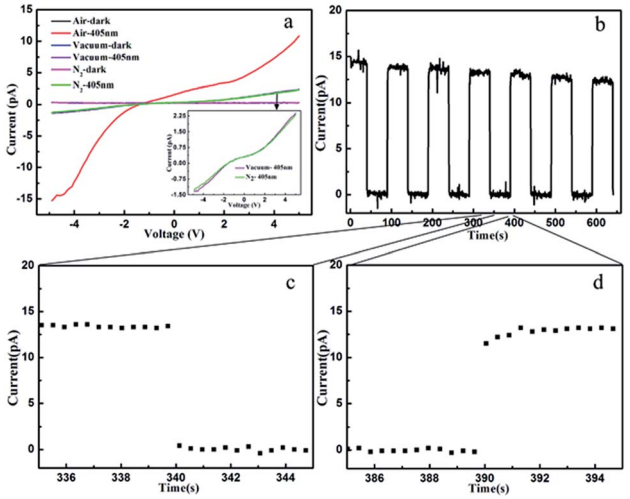

Fig. 4 (a) The I–V curves of an HfS_3 nanobelt photodetector under 405 nm light illumination measured in vacuum, nitrogen and air conditions, respectively. The inset is local amplification figure. (b) The reproducible on/off switching of the photodetector upon 405 nm light illumination. (c and d) The enlarged portion of a 335–345 s range and a 385–395 s range corresponding to decay time and rise time, respectively.

result can support the trapping mechanism previously proposed for p-type semiconducting photodetectors.[21] As we all know, the holes are dominant carriers in p-type HfS_3 nanobelt.[22] Because the width and the thickness of the nanobelt are rather small, it is lacking in carriers, leading to a low current in the dark state.[23] Under illumination in ambient conditions, however, the nanobelts absorbed photons and generated electron–hole pairs. Meanwhile, oxygen molecules were adsorbed onto the nanobelt surface and captured free electrons from the nanobelt in line with a scheme $[O_2(g) \rightarrow O_2(ad); O_2(ad) + e^- \rightarrow O_2^-]$.[21] Due to the disappearance of electrons, the holes concentration in the nanobelt surface increased. Therefore, the conductivity of the HfS_3 nanobelt increased, resulting in the dramatic increase of photocurrent. Under vacuum or nitrogen condition, oxygen adsorption becomes rare. Therefore, the concentration of holes is lower in vacuum or nitrogen than that in air, considering that oxygen acts as a trap for electrons. This explained the weakening of photocurrent in the vacuum or nitrogen.

The time response of HfS_3 nanobelt photodetector is shown in Fig. 4b, which was measured by periodically switching a 405 nm light on and off at an applied voltage of −5.0 V. Clearly, the photodetector showed reversible switching between low and high conductance states with good stability and reproducibility. The dark current of the photodetector is 0.04 pA, and the high photoresponse of 1.2 mW cm^{-2} is found under irradiation with 405 nm light. The ratio of photocurrent-to-dark current (on/off ratio) is about 337.5. The time taken for the current to increase from 10% to 90% of the peak value, or *vice versa*, are defined as the rise time and decay time, respectively.[24] As shown in Fig. 4c and d, we can see that the rise time and decay time was faster than the limit of our measurement setup (0.4 s). To assess the efficiency of an electron transport and carrier collection, both responsivity and quantum efficiency were calculated. The

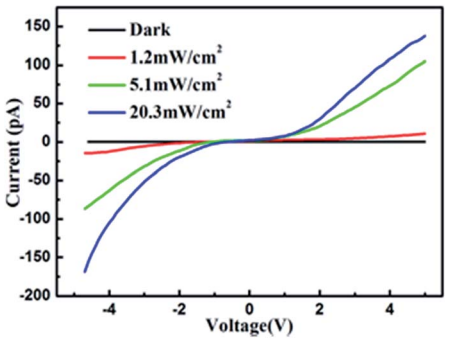

Fig. 5 Typical I–V characteristics of HfS_3 nanobelt photodetector illuminated with different power and dark condition.

responsivity (R_λ) and quantum efficiency (QE) can be determined from the following equations:

$$R_\lambda = \Delta I/PS$$

$$\mathrm{QE} = hcR_\lambda/e\lambda$$

where ΔI is the difference between the photoexcited and dark current, P is the light power density irradiated on the individual nanobelt, S is the area of the nanobelt, λ is the exciting wavelength, h is Planck's constant, c is the velocity of the light, and e is the electronic charge. Based on the above values, R_λ and QE of the present nanobelt are 0.11 A W^{-1} and 30% at an applied voltage of −5 V, respectively.

Typical I–V characteristics of HfS_3 nanobelt photodetector illuminated by 405 nm light with different powers (1.2 mW cm^{-2}, 5.1 mW cm^{-2} and 20.3 mW cm^{-2}) and in a dark condition is shown in Fig. 5. The Schottky barrier non-linear I–V behaviour obviously remains unchanged with increased light intensity. The photocurrent monotonously increased with increased light illumination intensity from a dark condition to 20.3 mW cm^{-2}. It disclosed that the hole carrier photo-generation efficiency is proportional to the absorbed photon flux.

Conclusions

In summary, for the first time, HfS_3-nanobelts were prepared and used as individual HfS_3-nanobelt FET and photodetectors. Electrical properties were investigated in the fabricated FET, from which the p-type semiconducting characteristic was revealed. The individual HfS_3-nanobelt photodetector has an ultralow dark current of 0.04 pA and a large on/off ratio (337.5) illuminated by 405 nm light with 1.2 mW cm^{-2}. It demonstrated excellent stability and sensitivity to 405 nm light. The responsivity and the quantum efficiency were estimated to be 0.11 A W^{-1} and 30%, respectively. The totality of the above results suggest that the HfS_3 nanobelts are promising for nanoscale electronic and optoelectronic devices. We believe that the research will allow the recognition of a high performance HfS_3-nanobelt and will play a positive role in nanodevice with 1D transition-metal trichalcogenide nanostructure.

Experimental section

Material preparation and characterization

HfS_3 nanobelts were directly synthesized by a chemical vapor transport method. In a typical procedure, first, a hafnium powder (99.9%, 173.8 mg) and sulfur sublimate powder (99.9%, 95.9 mg) were completely mixed according to the stoichiometric ratio (1 : 3). Then, the mixture was sealed in a quartz tube under vacuum (Φ 6 mm $\times$ 10 mm, *ca.* 10^{-2} Pa) and was placed in a conventional horizontal furnace (temperature gradient: *ca.* 10 K cm^{-1}) with the powders positioned at the center of the furnace. After the furnace was keep at 650 °C for 10 h, the HfS_3 nanobelts were obtained on the inner surface of the tubes. The morphology, structure, composition and UV-vis absorption of the samples were determined by X-ray diffraction with Cu Kα radiation (XRD, Shimadzu XRD-6000), field-emission scanning electron microscopy (SEM, Hitachi S-4800) with an energy-dispersive X-ray spectrometer (EDX), High-resolution transmission electron microscopy (HRTEM, JEOL2010), and UV-3600 spectrophotometer (Shimadzu UV-3600).

Fabrication of FET device and photodetectors

Appropriate amounts of HfS_3 nanobelts were suspended in ethanol by sonication for 5 min, and then a drop of this dispersion was dried on an oxidized Si wafer substrate with a 300 nm thick SiO_2 top layer that serves as a gate oxide. The standard photolithography technique was used to design the source and drain electrodes by Ti/Au (10/100 nm) metal evaporation and a lift-off procedure. Various gate voltages were applied to the Si substrate to determine the field-effect curves in the standard global back-gate geometry. The current–voltage (*I–V*) characteristics of the nanobelt photodetector were measured by Model CRX-4K Cryogenic Probe Station (Lake Shore Inc.) and Keithley 2636A (Keithley Instruments Inc.). For photodetector fabrication, the FET device without gate voltage was illuminated with a light of different wavelengths in vacuum, nitrogen and air condition, and the photocurrent was also recorded using Keithley 2636A. The spectral response for wavelengths was recorded using a different wavelength laser device.

Acknowledgements

We greatly appreciate the financial support from National Natural Science Foundation of China (NSFC) (no. 21171091) and the support from 973 Program (no. 2011CB933502, 2007CB936404).

Notes and references

1 L. Bian, X. W. Zhang, C. Y. Luan, Z. P. Juan Antonio, X. Z. Zhang, Y. M. Wu and J. S. Jie, *J. Mater. Chem. A*, 2013, **1**, 6313.
2 L. Wang, M. Lu, X. G. Wang, Y. Q. Yu, X. Z. Zhao, P. Lv, H. W. Song, X. W. Zhang, L. B. Luo, C. Y. Wu, Y. Zhang and J. S. Jie, *J. Mater. Chem. A*, 2013, **1**, 1148.
3 M. D. Wang, C. C. Xing, K. Cao, L. Zhang, J. B. Liu and L. Meng, *J. Mater. Chem. A*, 2014, **2**, 9496.
4 G. L. Frey, R. Tenne, M. J. Matthews, M. S. Dresselhaus and G. Dresselhaus, *J. Mater. Res.*, 1998, **13**, 2412.
5 A. Sengupta and S. Mahapatra, *J. Appl. Phys.*, 2013, **113**, 194502.
6 X. C. Wu, Y. R. Tao and Q. X. Gao, *Nano Res.*, 2009, **2**, 558.
7 X. C. Wu, Y. R. Tao and Q. X. Gao, *Chem. Commun.*, 2009, **40**, 6008.
8 Y. Q. Liu, M. Zhang, F. X. Wang and G. B. Pan, *J. Mater. Chem. C*, 2014, **2**, 240.
9 X. F. Wang, Z. Xie, H. T. Huang, Z. Liu, D. Chen and G. Z. Shen, *J. Mater. Chem.*, 2012, **22**, 6845.
10 R. M. Ma, L. Dai, H. B. Huo, W. Q. Yang, G. G. Qin, P. H. Tan, C. H. Huang and J. Zheng, *Appl. Phys. Lett.*, 2006, **89**, 203120.
11 L. Li, H. Lu and K. M. Deng, *J. Mater. Chem. A*, 2013, **1**, 2089.
12 E. Canadell, C. Thieffry, Y. Mathey and M. H. Whangbo, *Inorg. Chem.*, 1989, **28**, 3043.
13 H. Jin, D. Cheng, J. X. Li, X. J. Cao, B. X. Li, X. F. Wang, X. Y. Liu and X. D. Zhao, *Solid State Sci.*, 2011, **13**, 1166.
14 A. Zwick, G. Landa, M. A. Renucci and R. Carles, *Phys. Rev. B: Condens. Matter Mater. Phys.*, 1982, **26**, 5694.
15 X. C. Wu, Y. R. Tao and Q. X. Gao, *Nano Res.*, 2009, **2**, 558.
16 X. C. Wu, Y. R. Tao, Q. X. Gao, C. J. Mao and J. J. Zhu, *Chem. Commun.*, 2009, **28**, 4290.
17 L. Li, X. S. Fang, T. Y. Zhai, U. K. Gautam, X. C. Wu, Y. Koide, Y. Bando and D. Golberg, *Adv. Mater.*, 2010, **22**, 4151.
18 L. Li, H. Q. Wang, X. S. Fang, T. Y. Zhai, Y. Bando and D. Golberg, *Energy Environ. Sci.*, 2011, **4**, 2586.
19 L. B. Luo, X. B. Yang, F. X. Liang, J. S. Jie, Q. Li, Z. F. Zhu, C. Y. Wu, Y. Q. Yu and L. Wang, *CrystEngComm*, 2012, **14**, 1942.
20 K. Deng and L. Li, *Adv. Mater.*, 2014, **26**, 2619.
21 C. L. Hsu, H. H. Li and T. J. Hsueh, *ACS Appl. Mater. Interfaces*, 2013, **5**, 11142.
22 B. Mukherjee, E. S. Tok and C. H. Sow, *J. Appl. Phys.*, 2013, **114**, 134302.
23 C. Soci, A. Zhang, B. Xiang, S. A. Dayeh, D. P. R. Aplin, J. Park, X. Y. Bao, Y. H. Lo and D. Wang, *Nano Lett.*, 2007, **7**, 1003.
24 W. Tian, C. Zhang, T. Y. Zhai, S. L. Li, X. Wang, J. W. Liu, X. Jie, D. Q. Liu, M. Y. Liao, Y. Koide, D. Golberg and Y. Bando, *Adv. Mater.*, 2014, **26**, 3088.